International Journal on Science and Technology (IJSAT)
E-ISSN: 2229-7677 ● Website: www.ijsat.org ● Email: editor@ijsat.org

Theoretical Testing of Varying Material Mass Impact on Ballistic Performance of UAV-Deployed Spherical Payloads

Sreehari Kambrath [1], Sneha P.S [2]

[1] Assistant Manager, Aircraft Engine Health Monitoring, Genpact India Pvt Ltd
[2] Flight Data Integration Analyst, Aircraft Engine Health Monitoring, Genpact India Pvt Ltd

Abstract
This study presents a theoretical analysis into the influence of material mass on the ballistic performance of spherical payload samples of three main aerospace-grade materials, including AL 8090, Ti-6Al-4V, Zircaloy-4 deployed from unmanned aerial vehicles (UAVs) across an operational altitude range of 30 to 1000 meters. The diameter of the spherical payload bomb for selected materials are taken as 260 mm for better idealization and area uniformity. The analysis employs classical free-fall dynamics and numerical integration techniques to evaluate key impact parameters such as time of descent, velocity, and momentum. The impact time computation is executed through a simple python-based program for avoiding the complexities in calculation. Based on the computed magnitudes, different aerospace materials are assessed and comparatively classified according to their suitability for various applications, including military, safety, and hybrid payload delivery systems. The study outcomes indicate that material selection significantly affects descent time, terminal velocity, and drag efficiency, with denser materials exhibiting lower drag to weight ratios and enhanced momentum characteristics. The findings support optimized material choice for applications in military delivery systems, hybrid fire suppression payloads, and safety modules deployed via UAV platforms.

Keywords: ballistic performance, aerospace materials, UAV payload deployment.

1. Introduction

Unmanned Aerial Vehicles (UAVs) have revolutionized modern payload delivery systems, offering precision, flexibility, and reduced operational risks in military, humanitarian, and scientific applications. Among various payload configurations, spherical payloads are particularly advantageous due to their inherent aerodynamic stability, structural resilience, and predictable ballistic behavior. Unlike irregularly shaped payloads, spheres exhibit uniform air resistance and stress distribution, ensuring consistent flight dynamics during free-fall deployment and makes them suitable to conduct experimental and theoretical studies. Theoretical and experimental work carried out by Lu et al., (2025) presents the concept of ballistic studies in UAV systems [1]. The present attempt mainly focuses on the theoretical analysis of varying material mass impact on the ballistic performance of UAV-deployed spherical payloads, aiming to optimize their design for enhanced accuracy, impact resistance, and mission success [16],[20]

1.1 Role and Advantages of Spherical Payloads in UAV Deployment

Spherical payloads are extensively employed in UAV operations due to their geometric efficiency. Their symmetrical shape minimizes drag-induced deviations, allowing for more stable and controlled descent trajectories [7]. This is particularly crucial in precision airdrop systems, where payloads must land within designated zones without any damage. Some of the common examples include: Emergency supply delivery like medical kits, food, and survival gear in disaster zones.
Military and defense applications (deploying sensors, flares, or reconnaissance devices), Scientific and environmental monitoring (weather balloons, atmospheric sensors, or agricultural dispersants).
The spherical geometry ensures that, regardless of orientation during descent, the payload maintains consistent aerodynamic properties, reducing the risk of tumbling or erratic flight paths.
The choice of a spherical payload is supported by fundamental principles of fluid dynamics and structural mechanics [20]. Unlike cubic or irregular shapes, spheres experience uniform drag distribution, preventing unpredictable rotations that could compromise landing accuracy. Additionally, the absence of sharp edges reduces stress concentrations upon impact, enhancing durability. The research primarily reinforces the sphere's superiority by analyzing how material mass variations influences terminal velocity, ballistic impact characterization in payload survivability.

By studying how material mass affects ballistic behavior (e.g., kinetic energy dissipation, deformation modes), this research provides insights into optimizing payload design for high-impact resilience and reliable deployment.

2. Methodology

The methodology mainly focusses on key principles of motion of falling objects and free fall physics followed by consideration and non -consideration of the impact of drag forces.

Figure 1: Methodology

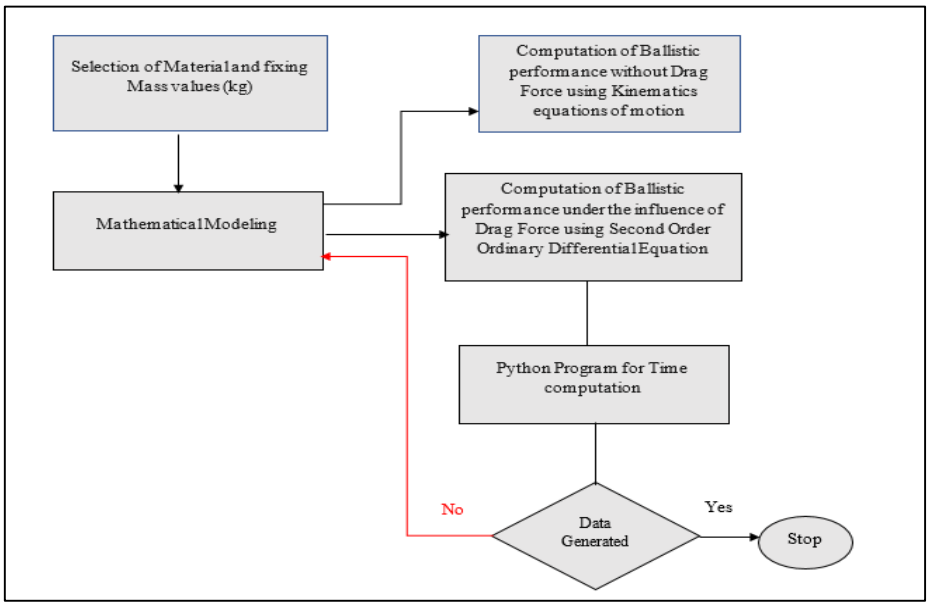

The theoretical studies are carried out for a typical medium altitude un-manned aerial having a payload capacity of 250kg and above, also the deployment of spherical payloads was carried out at a fixed altitude range of 30 to 1000metres from its any cruise point 'd' to 'e' as shown in Fig 2. which corresponds to a hovering position from selected point to the ground level to minimize the external compressibility effects that may result in the theoretical computation with better accuracy[15].

Figure 2: Flight Mission Profile of a typical UAV

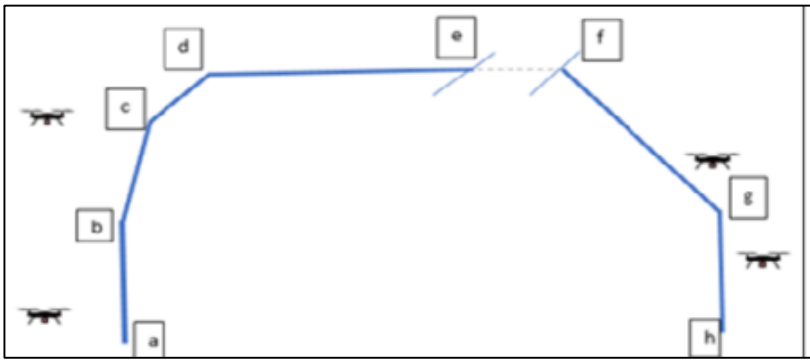

Flight Phase	Leg Reference
Initial Hovering	a to b
Takeoff	b to c
Climb	c to d
Cruise	d to e
Loiter	e to f
Descent	f to g
Landing	g to h

2.1 Material Selection

The payload material samples are selected accordingly as per the aerospace standards and their characteristics are mentioned in Table 1

Table 1: Selected Material Samples Payload (diameter (d) = 260mm)

Sl No	Sample	Density (kg/m^3)	Calculated Mass value (kg)
1	8090 AL-Li	2600	23.92
2	Ti-6Al-4V	4500	41.39
3	Zircaloy-4	6400	60.47

The alloys 8090 Al-Li (Aluminum-Lithium), Ti-6Al-4V (Titanium), and Zircaloy-4 (Zirconium) are all known extensively throughout the aerospace world for their strength-to-weight ratios, and because of this, they are perfect for applications where structural strength has to be achieved without excessive weight addition. This is an extremely important requirement throughout aerospace systems where each gram translates directly into performance and fuel economy [9],[11].

All three alloys have outstanding corrosion resistance, though in varying environments. 8090 Al-Li is resistant to atmospheric and marine corrosion, Ti-6Al-4V does very well even in chemically severe environments, and Zircaloy-4 has outstanding corrosion resistance in high-temperature steam and irradiation environment commonly employed in nuclear-related aerospace applications [14]
From a fatigue performance perspective, these materials are designed to resist cyclic loading and unloading, which is crucial in aerospace components like wings, fuselages, turbine blades, and landing gears that endure dynamic stresses during flight operations.

All these materials also exhibit satisfactory thermal stability, retaining their mechanical properties over a wide range of temperatures. While Ti-6Al-4V is capable of withstanding the high temperatures of jet engines, Zircaloy-4 operates well under thermal and radiation stress, and 8090 Al-Li retains good mechanical stability over moderate operating temperatures [10],[13].

Considering manufacturing viewpoint, these alloys are relatively workable and machinable and can be formed, welded, or processed by using standard aerospace manufacturing methods. While Ti-6Al-4V and Zircaloy-4 are difficult to machine compared to aluminum alloys, they are nevertheless extensively employed because of their performance advantages [13].

2.2 Mathematical Modeling

In order to analyze the ballistic performance of spherical payloads deployed from UAVs in terms of various aerospace materials (8090 Al-Li, Ti-6Al-4V, and Zircaloy-4), two modeling methods are employed: one without aerodynamic drag and the other including it through a second-order nonlinear differential equation which can be solved using integral calculus techniques. These models are designed to compute important performance parameters — time of descent, impact velocity, and ground impact momentum for different deployment altitudes.

2.2.1 Modeling using kinematic principles under free fall conditions

In the absence of aerodynamic drag force, the payload's motion is described with classical kinematic equations of uniformly accelerated motion. The major equations employed are the ones below and can be obtained utilizing simple kinematic equations of motions as shown below

- Theoretical Impact time
  The theoretical impact time, also known as the time of descent, refers to the total time taken by an object to fall from a specified height to the ground under the influence of gravity alone. Mathematically it is expressed in (1) ,

$$t = \sqrt{\frac{2H}{g}} \qquad (1)$$

where ‘t’ is the theoretical impact time in seconds (s), ‘H’ is the falling height in metres (m) and g is the acceleration due to gravitational field which is taken as 9.8 m/s^2. This computation is very much helpful in observing the trajectory of the falling object without the interference of external forces as shown in Fig. 3. [3],[20].
Figure 3: Trajectory of a freely falling body

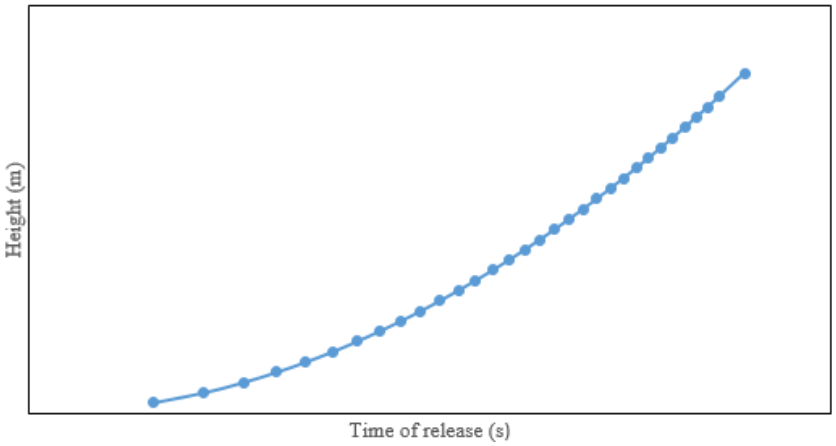

- Theoretical Impact Velocity
  The thoeretical impact velocity, also known as free-fall velocity, is the velocity of an object just before it hits the ground when falling under the influence of gravity alone, with no air resistance (idealized conditions). This velocity is the final velocity attained at the end of the fall, assuming the object starts from rest and accelerates uniformly due to gravity.

From kinematic equation of motion for a freely falling body the equation is depicted as [3]:

$$h = ut + \frac{1}{2}gt^2 \quad (2)$$

as the initial release velocity u is taken as zero then the equation reduces to (1). Therefore, on differentiating (1) with respect to 't' we retrieve the following

$$V = \frac{dH}{dt} = gt \quad (3)$$

Where 'V' is the theoretical impact velocity and can be written as V= gt , by substituting for 't' from (1) the following expression can be obtained

$$V = \sqrt{2gH} \quad (4)$$

The above kinematic expressions are taken into account under the assumption of the following consideration, that the body is at:

a) Constant gravitational acceleration field (g)
b) Zero initial vertical velocity (i.e., the object is released, not thrown)
c) No other external forces acting, such as drag or lift or even the buoyant forces.

2.2.2 Modeling using Second Order Non-Linear Differential equations

The mathematical modeling is implemented by adopting basic Newton's laws of motion. The concept of net force effect is taken into account to solve the fall dynamics under the consideration of drag force. The basic free body diagram for deployment is as shown in below Fig 3.

Figure 3: Free body diagram of Payload mass deployment from UAV

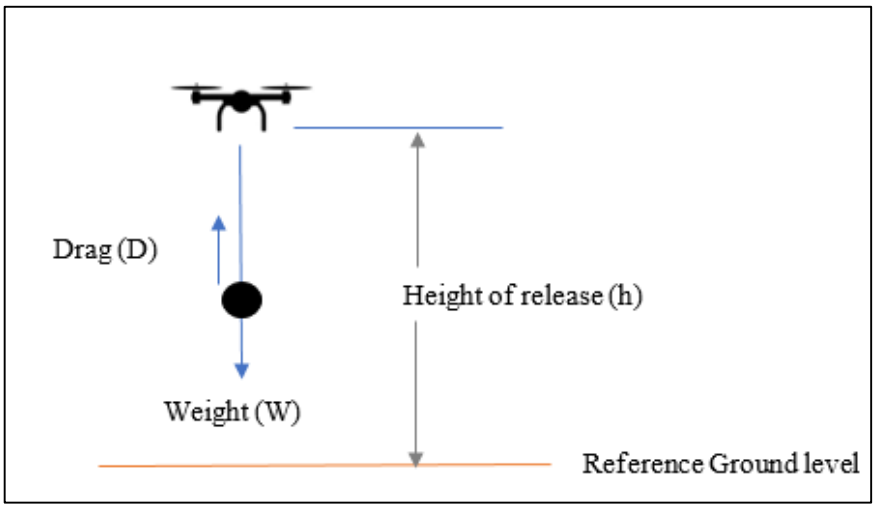

From Fig.3 the equations of motion for the particular system is expressed through the law of equilibrium of forces, but here the total forces including the net force is taken to be zero for getting a feasible model The equations are modeled based on the work carried out by Kalimullah et al., (2006) for falling bodies and the experiment performed by Hassanain (2014) for free fall balls [18],[19].

$$F_{net} = W - D \quad (5)$$

Here F_{net} is $m\frac{dV}{dt}$ that is incorporated in the below expression, m is the payload mass and V is the falling velocity

$$m\frac{dV}{dt} = mg - \frac{1}{2}\rho V^2 S C_D \quad (6)$$

Dividing throughout by 'm' we get $\frac{dV}{dt} = g - \frac{1}{2m}\rho V^2 S C_D$ (7)

The notations represent the usual meaning as per fluid dynamics concept but its effective to recall the terms once again as ρ represents the fluid density, S represents the exposed cross-sectional area and C_D is the drag coefficient, which is taken as a fixed value of 0.47 for spherical payloads [12],[17]

Here we introduce a new term called inverse ballistic coefficient represented by k This parameter will serve serving as a drag scaling factor that governs the influence of aerodynamic resistance on the payload's descent [21]. A lower value indicates more ballistic-like behavior, with reduced drag deceleration and higher impact velocities. Also, it's important to note that the term Φ is a function of fluid density and ballistic coefficient ß which can be denoted as

$$k = F(\rho, ß^{-1}) \quad (8)$$

As the compressibility effects are assumed negligible therefore the density remains constant for the fluid having the value of 1.22kg/m^3. It is important to note that based on Stoke's law the object immersed in a

fluid while falling will meet the condition of terminal velocity which is defined as the velocity at which the object weight balances the drag force [5],[6]. Mathematically expressed as

$$\frac{1}{2}\rho V^2 S C_D = mg \quad (9)$$

Therefore, terminal velocity, $V_t = \sqrt{\frac{2mg}{\rho S C_D}} = \sqrt{\frac{g}{k}}$ (10)

The expression (7) can be re-written as $\frac{dV}{dt} = g - kV^2$ (11)

The fall velocity can be in expressed interms of release height or operating altitude 'h' and (11) can be formulated as second order ordinary differential equation as shown in (12)

$$\frac{d^2h}{dt^2} + k\left(\frac{dh}{dt}\right) - g = 0 \quad (12)$$

Through suitable boundary conditions the payload at rest therefore $V = 0$, $t = t_i$ also $\frac{dV}{dt} = 0$, $t = t_f$. The ratio of $\frac{t_i}{t_f}$ <<1 which implies the initial time release is negligibly small. The expression (12) can be solved through the me mentioned boundary conditions and yield the following generalized expressions for impact time and impact velocity, which is taken further for performing ballistic computations.

$$t = \frac{1}{\sqrt{gk}}\cosh^{-1}(e^{kh}) \quad (13)$$

$$V(t) = \sqrt{\frac{g}{k}}\tanh(t\sqrt{gk}) \quad (14)$$

The time data computation for the spherical payloads with different values of k for the required material payload samples is proven to be a tedious process as it involves inverse hyperbolic functions, this can be simplified by developing a math-based python computation program code to generate the values accordingly to increase precision and accuracy for operating altitude range from 30 to 1000 m [8].

Figure 4: Python Computation Program for Impact Time

```
# Heights list
heights = [
    30, 60, 90, 120, 150, 180, 210, 240, 270, 300,
    330, 360, 390, 420, 450, 480, 510, 540, 570, 600,
    630, 660, 690, 720, 750, 780, 810, 840, 870, 900,930,1000
]

# Time function
def fall_time(h):
    return (1 / math.sqrt(g * k)) * math.acosh(math.exp(k * h))

# Prepare data
data = {'Height (m)': heights, 'Time to Fall (s)': [fall_time(h) for h in heights]}

# Create DataFrame
df = pd.DataFrame(data)

# Display the table
print(df.to_string(index=False))

# Save to Excel
df.to_excel("fall_times_k_00063.xlsx", index=False)
print("\nExcel file 'fall_times_k_00063.xlsx' has been saved.")
```

The basic fluidic interaction with the spherical payload surface can be quantified using the magnitude of Reynolds number 'Re' which signifies the fluid exposure is laminar or turbulent through conditions $\frac{\rho V(t)d}{\mu} < 2400$ and $\frac{\rho V(t)d}{\mu} > 10^5$ respectively [2],[12],[17]. The impact of the falling body can be conveniently analyzed through the basic momentum equation 'p' as shown below:

$$p = mV(t) \quad (15)$$

3. Results and Discussion

The difference in impact time due to atmospheric drag was assessed for spherical payloads made of Al 8090, Ti-6Al-4V, and Zircaloy-4, compared against idealized free-falling behavior. All materials were found to have higher impact times under drag, with Ti-6Al-4V and Zircolay-4 falling the fastest, then Al 8090.The payload made of material with the highest density shows the shortest impact time for the release heights as depicted in Fig. 5. The growing delay noted for the lower-density materials indicates increased sensitivity to drag. These findings underscore material choice in applications where descent velocity and momentum are paramount, including UAV payload drop or ballistic impact systems

Figure 5: Variation Impact time with release height

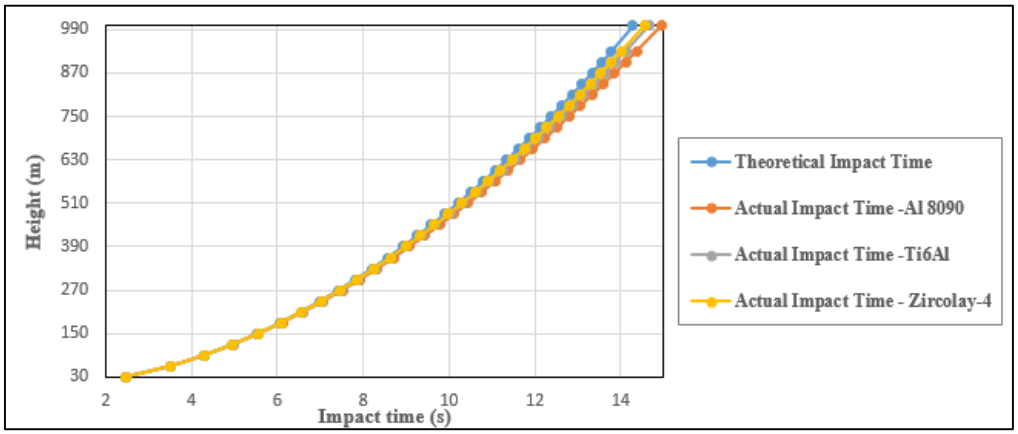

Figure 6: Variation of Drag Forces with Height

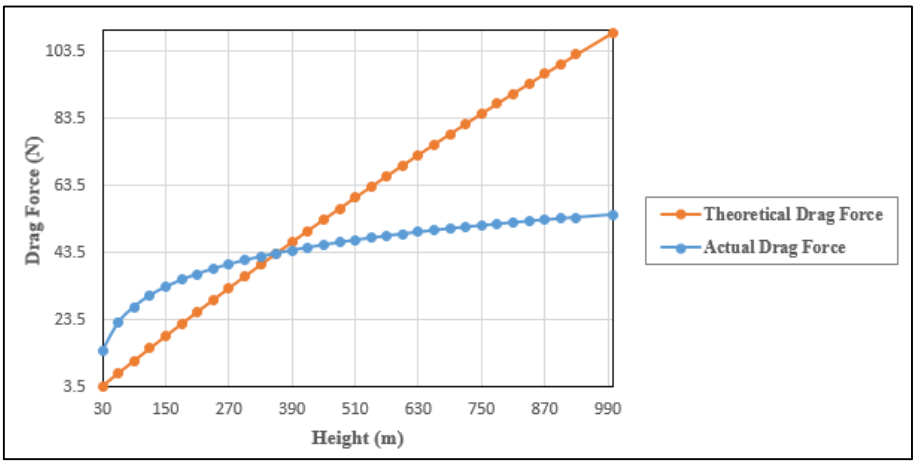

As per the data analysis the theoretical drag force rises with height, with constant velocity and drag coefficient scaling with air density as per Fig.6. The actual drag force also increases initially but levels off above 500 m. This deviation is caused by the reality that real drag is dynamically influenced by reducing air density and the consequential increase in velocity in free fall [4]. When the object speeds up, reduced air density with increased altitude diminishes the overall growth of drag, leading to a saturation curve. The findings demonstrate the non-linear behavior of drag for realistic conditions of descent, and reinforce the necessity of altitude-sensitive modeling during the assessment of aerodynamic forces in UAV-delivered payloads.

The variation of drag-to-weight (D/W) ratio as a function of altitude for spherical payloads of Al 8090, Ti-6Al-4V, and Zircaloy-4 were assessed as per Fig.7. It is observed that the D/W ratio increases with altitude for all three materials because of the increase in drag force over fixed gravitational weight while accelerating downward. Al 8090 has the highest D/W ratio at all altitudes, being followed by Ti-6Al-4V and Zircaloy-4. The trend is in accordance with their material densities which reveals and validates the fundamental laws of falling physics and depicts a valuable insight that lower-density materials have proportionally greater drag forces, leading to greater D/W ratios. The trend emphasizes the aerodynamic penalty of low-density materials for descent applications, as higher D/W ratios correspond to greater deceleration and increased time to impact.

Figure 7: Drag to Weight Ratio for Payload Material Samples

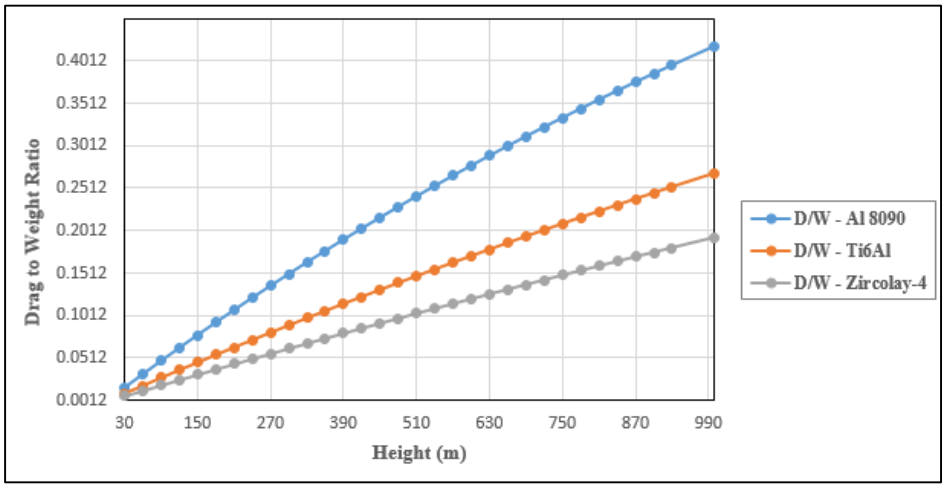

Figure 8: Study of Reynolds Number with height

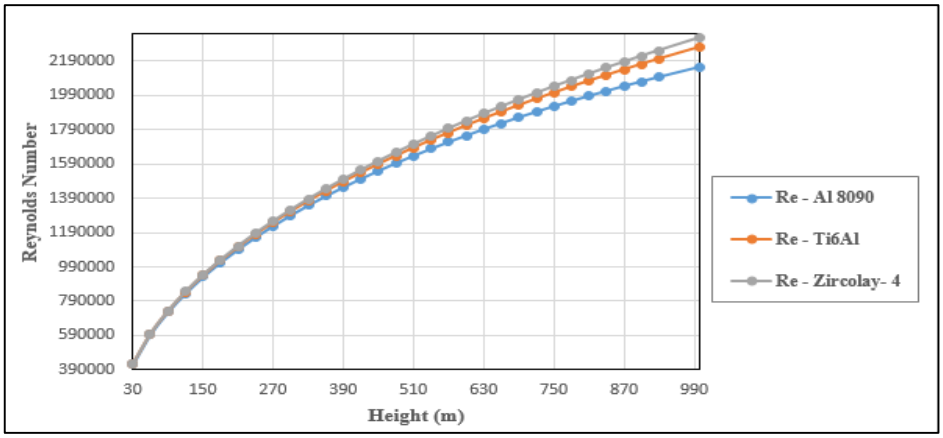

The consistently turbulent flow regime suggests that drag coefficients are relatively stabilized and not subject to laminar-to-turbulent transition effects, which would otherwise introduce variability. The Re values are comparable between materials because of equal geometries and similar initial-stage velocities. With further descent, minor differences arise, with Zircaloy-4 having the highest Reynolds number, followed by Ti-6Al-4V and then Al 8090 based on Fig.8. These are due to mass-dependent acceleration, where heavier materials have greater terminal velocities, hence resulting in higher Reynolds numbers indicating the flow experienced is turbulence having magnitude greater than 10^5.

Momentum is computed as the product of mass and instantaneous velocity based on (15), incorporating the effects of atmospheric drag throughout descent. Through a proper curve fitting momentum is plotted as an exponential function of time for each material impact as shown in Fig.9.All the materials show an exponential growth in momentum with time, as expected under gravity sustained acceleration as indicated in Fig.9. Zircaloy-4 has the highest value of momentum, followed by Ti-6Al-4V and Al 8090, due to the effect of material density and associated mass. It is appreciated that the nature of the curves and sustained growth in momentum shows that no payload attained terminal velocity within the descent window. Terminal velocity is usually characterized by the condition of equilibrium mg = D, where net acceleration vanishes. But throughout all altitudes examined, the drag force was always below the gravitational force, thus causing the system to never reach a steady-state fall. This is evidenced by the rising Reynolds numbers and the lack of flattening of the drag force plots. These results support that, for the considered height interval (30–1000 m), the objects were in a pre-terminal phase of acceleration, leading to ever-growing velocity and momentum for a high payload mass.

Figure 9: Momentum as a function of Impact time

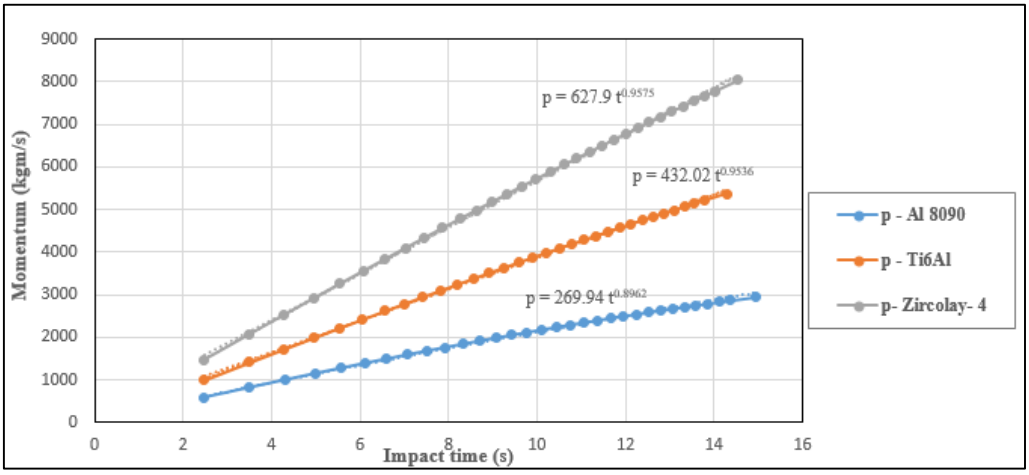

Ballistic performance across altitudes from 30 to 1000 m reveals that Zircaloy-4 exhibits the highest terminal velocities (132.82 m/s) and momentum (8030.80 kg·m/s), attributed to its low drag coefficient. k=0.00010716 and minimal D/W ratio based on Table.2. In contrast, 8090 Al-Li shows the lowest momentum and highest D/W ratio, indicating greater deceleration due to drag. Ti-6Al-4V provides intermediate performance. Across all materials, increasing velocity and momentum with altitude confirm that terminal velocity was not achieved within the theoretical tested range, highlighting continued acceleration and the dominance of mass over drag resistance in short-duration ballistic descent.

Table 2 : Ballistic Performance based on Altitude ranging between 30 to 1000 metres

Sl No	Payload	k	V(t) (m/s)	p (kgm/s)	D/W ratio
1	8090 AL-LI	0.000270901	24.15 to 123.00	577.67 to 2942.38	0.0161 to 0.4182
2	Ti-6Al-4V	0.000156558	24.19 to 129.75	1001.28 to 5369.91	0.00934 to 0.2688
3	Zircaloy-4	0.00010716	24.20 to 132.82	1463.96 to 8030.80	0.00640 to 0.1929

4. Conclusion

The theoretical testing of ballistic performance based on the deceleration constant k, velocity, momentum, and drag-to-weight ratio indicates that Zircaloy-4, with the lowest k value, offers the best descent performance under ideal free-fall conditions. Its superior aerodynamic efficiency and high momentum delivery make it well-suited for high-impact defense applications, particularly where nuclear or strategic payloads are involved and cost is a secondary consideration. Ti-6Al-4V, exhibiting a moderate k value, provides a strong balance between performance and drag resistance, making it ideal for general-purpose UAV-deployed kinetic payloads and precision-guided systems where both effectiveness and cost-efficiency are essential. On the other hand, 8090 Al-Li, with the highest k value and greater sensitivity to aerodynamic drag, is more appropriate for low-mass, short-range delivery systems or cost-sensitive applications, such as expendable surveillance or sensor payloads. It is important to emphasize that these insights are derived from theoretical modeling under idealized atmospheric and geometric conditions. In actual operational environments, external factors such as turbulence, wind shear, boundary layer effects, and thermal variations can significantly influence the descent characteristics. Therefore, while the results provide valuable baseline comparisons, experimental validation under controlled real-world conditions is essential for deployment-level accuracy. From a material cost perspective, Ti-based alloys offer an optimal trade-off between ballistic performance and affordability for most operational scenarios. Although Zircaloy-4 delivers superior performance, its higher cost restricts its use to specialized, high-priority military applications where performance requirements outweigh economic constraints.

References

1. Lu Z, Wang Z, Yao S, Zhong M, Liu K, Wang J. Theoretical and experimental studies on the interior ballistic of large UAV ejection based on trifluoromethane phase transition. Sci Rep. 2025 Feb 8;15(1):4794. doi: 10.1038/s41598-025-89273-w
2. Alam, Firoz & Steiner, Tom & Chowdhury, Harun & Moria, Hazim & Khan, Iftekhar & Aldawi, Fayez & Subic, Aleksandar. (2011). A study of golf ball aerodynamic drag. Procedia Engineering. 13. 226-231. 10.1016/j.proeng.2011.05.077.
3. Sivaraj, Priyadharsini. (2018). A Study on Motion of a Free-Falling Body in Kinematic Equation. International Journal for Research in Applied Science and Engineering Technology. 6. 3118-3124. 10.22214/ijraset.2018.1431.

4. Horvat, Dubravko & Jecmenica, Radomir. (2016). The free fall experiments. Resonance. 21. 259-275. 10.1007/s12045-016-0321-9.
5. Auerbach, David. (1988). Some limits to Stokes' law. American Journal of Physics - AMER J PHYS. 56. 850-851. 10.1119/1.15442
6. xu, Bin & Huang, Ning & He, Wei & Chen, Youxing. (2017). Investigation on terminal velocity and drag coefficient of particles with different shapes. Journal of Physics: Conference Series. 822. 012047. 10.1088/1742-6596/822/1/012047.
7. Leško, Jakub & Andoga, Rudolf & Breda, Robert & Hlinková, Miriam & Fozo, Ladislav. (2023). Flight phase classification for small unmanned aerial vehicles. Aviation. 27. 75-85. 10.3846/aviation.2023.18909.
8. Junfeng, Chen & Li, Hao & Ai, Ke & Shi, Zhengxuan & Xiao, Xiangpeng & Yan, Zhijun & Liu, Deming & Shum, Perry & Sun, Qizhen. (2024). Low-Altitude UAV Surveillance System via Highly Sensitive Distributed Acoustic Sensing. IEEE Sensors Journal. PP. 1-1. 10.1109/JSEN.2024.3452072.
9. Liang, Guofeng & Huang, Jiawen & Zhou, Dapeng & Li, Xiaojie & Li, Kebin & Zhu, Guichun & Liu, Zhongshu & Chen, Xiang & Hu, Jianian. (2024). Study on Explosive Welding of A7075/A1060/Ti-6Al-4V and Its Mechanical Properties. JOM. 77. 10.1007/s11837-024-06950-3.
10. Selmi, Noureddine & Sari, Ali. (2013). Study of Oxidation Kinetics in Air of Zircaloy-4 by in Situ X-Ray Diffraction. Advances in Materials Physics and Chemistry. 03. 168-173. 10.4236/ampc.2013.32023.
11. R., Leo Bright Singh & Jinu, G. & .M, Manoj & A., Elaya. (2022). Tribological Behaviour of Al8090-SiC Metal Matrix Composites with Dissimilar B4C Addition. Silicon. 14. 1-14. 10.1007/s12633-021-01608-0.
12. Bailey, A. B., and Hiatt, J., “Sphere Drag Coefficients for a Broad Rangeof Mach and Reynolds Numbers,” AIAA Journal, Vol. 10, No. 11, 1972,pp. 1436–144. https://doi.org/10.2514/3.50387
13. Shinhyo Bang, Ho-a Kim, Jae-soo Noh, Donguk Kim, Kyunghwan Keum, Youho Lee,Temperature-dependent axial mechanical properties of Zircaloy-4 with various hydrogen amounts and hydride orientations,Nuclear Engineering and Technology,Volume 54, Issue 5,2022, Pages 1579-1587,ISSN 1738-5733,https://doi.org/10.1016/j.net.2021.11.007.
14. Modi, Sita & Jha, Kailash. (2024). A Comparative Investigation on Mechanical and Electrochemical Characteristics of Annealed Ti-6Al-4V ELI with Other Grades of Titanium Alloys. Journal of Materials Engineering and Performance. 10.1007/s11665-024-10190-6.
15. Mohsan, Syed Agha Hassnain & Othman, N.Q.H. & Yanlong, Li & Alsharif, Mohammed & Khan, Muhammad. (2023).Unmanned aerial vehicles (UAVs): practical aspects, applications, open challenges, security issues, and future trends. Intelligent Service Robotics.16. 109-13710.1007/s11370-022-00452-4.
16. Raghav, K. & Karthik, T. & Kulkarni, S & Kumar, H.. (2025). Unmanned Aerial Vehicle (UAV) with Heavy Payload Capacity and Enhanced Stability. 10.1007/978-981-96-1158-4_16.
17. Nie, Deming & Wang, Jingwen & Li, Siwen & Lin, Jianzhong. (2024). Freely rising or falling of a sphere in a square tube at intermediate Reynolds numbers. Journal of Fluid Mechanics. 1000. 10.1017/jfm.2024.1004.
18. Kalimullah, & Garg, Madhur & Palakkandy, Arun. (2006). Motion of falling object.

19. Hameed, Hassanain. (2014). Invesatigation the Effect of Size and Weight on Drag Coefficient for Free Falling of Balls. Kufa Journal of Engineering. 2. 40-53. 10.30572/2018/KJE/211292.
20. Siva Sivamani Ganesh Kumar, Abhishek Gudipalli, A comprehensive review on payloads of unmanned aerial vehicle,The Egyptian Journal of Remote Sensing and Space Sciences,Volume 27, Issue 4,2024,Pages 637-644,ISSN 1110-9823,https://doi.org/10.1016/j.ejrs.2024.08.001.
21. F. Kumru, E. Altuntas and T. Akça, "Ballistic coefficient learning based impact point prediction of ballistic targets," 2018 26th Signal Processing and Communications Applications Conference (SIU), Izmir, Turkey, 2018, pp. 1-4, doi: 10.1109/SIU.2018.8404802.